Ultrahigh-spin spectroscopy of ^{159,160}Er: Observation of triaxial strongly deformed structures

J. Ollier and J. Simpson
STFC Daresbury Laboratory, Daresbury, Warrington WA4 4AD, United Kingdom

X. Wang, M. A. Riley, A. Aguilar, and C. Teal
Department of Physics, Florida State University, Tallahassee, Florida 32306, USA

E. S. Paul, P. J. Nolan, M. Petri,* S. V. Rigby, J. Thomson, and C. Unsworth
Oliver Lodge Laboratory, University of Liverpool, Liverpool L69 7ZE, United Kingdom

M. P. Carpenter, R. V. F. Janssens, F. G. Kondev, T. Lauritsen, and S. Zhu
Nuclear Engineering Division and Physics Division, Argonne National Laboratory, Argonne, Illinois 60439, USA

D. J. Hartley
Department of Physics, U. S. Naval Academy, Annapolis, Maryland 21402, USA

I. G. Darby†
Department of Physics and Astronomy, University of Tennessee, Knoxville, Tennessee 37996, USA

I. Ragnarsson
Division of Mathematical Physics, LTH, Lund University, Post Office Box 118, S-22100 Lund, Sweden
(Received 19 October 2009; published 29 December 2009)

Three weakly populated high-spin rotational bands associated with the γ decay of ^{159}Er and ^{160}Er were observed in fusion-evaporation reactions involving a beam of ^{48}Ca at an energy of 215 MeV incident on a ^{116}Cd target. The γ decays were detected using the highly efficient Gammasphere spectrometer. The discovery of these bands, which extend discrete-line spectroscopy in these nuclei to ultrahigh spin of $\sim 60\hbar$, is consistent with recent observations of high-spin collective structures in isotopes of Er, Yb, and Tm around $N = 90$. Cranked Nilsson-Strutinsky calculations suggest that these bands may arise from well-deformed triaxial configurations with either positive or negative γ deformation.

DOI: 10.1103/PhysRevC.80.064322 PACS number(s): 27.70.+q, 21.10.Re, 23.20.Lv

I. INTRODUCTION

Spectroscopic studies investigating the interplay between single-particle and collective structures at high angular momentum have led to the observation of many nuclear phenomena. A particularly fascinating region occurs in the rare-earth nuclei near $N = 90$, where dramatic changes in shape are found as the nucleus is excited to higher angular momentum values. The use of state-of-the-art γ-ray detector arrays now enables discrete-line spectroscopy to be performed to ultrahigh spin ($\sim 60\hbar$). This has led to the recent discoveries of rotational band sequences that appear to bypass the textbook band-terminating single-particle oblate states in ^{157,158}Er [1] in the $40\hbar$–$50\hbar$ range. These sequences represent a return to collective behavior for these nuclei at the highest spins.

The $A \sim 158$ Er isotopes lie between two distinct regions within the high-spin domain. There is a region of nuclei that exhibit superdeformed (SD) structures, which lies around ^{152}Dy [2], and a region where triaxial strongly deformed (TSD) structures have been inferred in ^{161,163,165,167}Lu [3–7]. Indeed, triaxial structures were established with the observation of "wobbling" excitations in ^{163}Lu [4,5]. Wobbling excitations are unique to rotating asymmetric nuclei [8] and had been predicted to occur at high spin for more than 30 years [9]. Interestingly, a study of high-spin states at the heavier edge of the SD mass 150 region revealed coexisting TSD and SD structures in ^{154}Er [10,11].

These observations led to searches for similar high-spin structures in other rare-earth nuclei between these two regions. This resulted in the observation of four weakly populated, high-spin rotational bands in ^{157,158}Er [1]. Notably, these bands have dynamic moments of inertia similar to the TSD structures in the Lu isotopes and in ^{154}Er. Cranked Nilsson-Strutinsky calculations suggest that these bands may also be associated with TSD structures. Moreover, the calculations suggest that the structures lie in a valley of favored shell energy in deformation and particle-number space [1].

A high-spin rotational band with a high moment of inertia characteristic of a TSD sequence has also been observed recently in the $N = 90$ nucleus ^{160}Yb [12]. In the Tm isotopes, high-spin bands, which may also correspond to triaxial-deformed shapes, have been reported in ^{160,161}Tm [13] and

*Present address: Nuclear Science Division, Lawrence Berkeley National Laboratory, Berkeley, California 94720, USA.

†Present address: Instituut voor Kern- en Stralingsfysica, Katholieke Universiteit Leuven, B-3001 Leuven, Belgium.

^{163}Tm [14]. Lifetime measurements, undertaken for the two rotational bands observed in ^{163}Tm [15], confirmed that these bands are associated with highly deformed structures with transition quadrupole moments of 7.4 and 7.7 *e* b, respectively. In addition, exploration of the high-spin structures of Hf isotopes has led to the discovery of deformed bands with high dynamic moments of inertia in $^{168,170-175}$Hf [16–20]. However, these bands appear to be associated with enhanced-deformed (ED) prolate shapes (deformations enhanced with respect to the normal deformed nuclear shapes) and SD structures [18], with the exception of the discovery of a possible TSD band in ^{168}Hf [16,21].

This recent body of data has revealed that the nature and understanding of the collective bands at ultrahigh spins changes rather rapidly with small variations in N and Z. The studies have revealed a complex mixture of SD, TSD, and ED structures. The present work was undertaken to search for high-spin rotational bands in ^{159,160}Er and three new bands with high dynamic moments of inertia are reported in these nuclei. The present article supercedes the conference proceedings [22,23] where these new band sequences were previously discussed.

II. EXPERIMENTAL DETAILS

High-spin states in ^{159,160}Er were populated using a 215-MeV beam of ^{48}Ca, which was incident upon enriched targets of ^{116}Cd, inducing fusion-evaporation reactions. The experiment was performed at the ATLAS facility at Argonne National Laboratory. The target consisted of two self-supporting ^{116}Cd foils with a total thickness of 1.3 mg/cm^2. The γ decays resulting from the reaction products were detected using the Gammasphere spectrometer [24]. A total of $\sim 1.9 \times 10^9$ events were collected when at least 7 of the 101 Compton-suppressed HPGe detectors fired in prompt coincidence. The data were collected over a 5-day period. Unfolding the events resulted in approximately 3.5×10^{10} quadruple and 1.4×10^{11} triple coincidence events, which were replayed off-line into RADWARE-format four-dimensional (E^4_γ) hypercubes and three-dimensional (E^3_γ) cubes for analysis [25].

III. RESULTS

Previous experimental work on $^{160}_{68}$Er$_{92}$ and $^{159}_{68}$Er$_{91}$ has established yrast and near-yrast normal-deformed rotational bands up to a spin of $\sim 50\hbar$ [26,27]. A search for rotational bands with high moment-of-inertia values was undertaken and three such sequences were found, two in ^{160}Er and one in ^{159}Er. The relative intensities of these bands were estimated to be of the order of 10^{-4} of the respective reaction channel yield, similar to the corresponding bands in ^{157,158}Er [1].

A γ-ray spectrum for the strongest of these bands in ^{160}Er (band 1) is presented in Fig. 1(b). This spectrum was produced from the cube (E^3_γ) using a sum of double gates set on all of the transitions in the band from 1017 to 1532 keV. In addition, two tentative transitions at 1593 and 1666 keV were observed. Figure 1(a) shows the low-energy range of a γ-ray spectrum produced with a sum of triple gates set on the transitions within this band generated from the hypercube (E^4_γ). Although no linking transitions between the new band and the normal-deformed, low-spin states could be established, yrast transitions of ^{160}Er are visible in Fig. 1(a). Transitions in ^{160}Er are also present in Fig. 1(b), labeled with an asterisk, at 938, 960, 983, and 1010 keV, which correspond

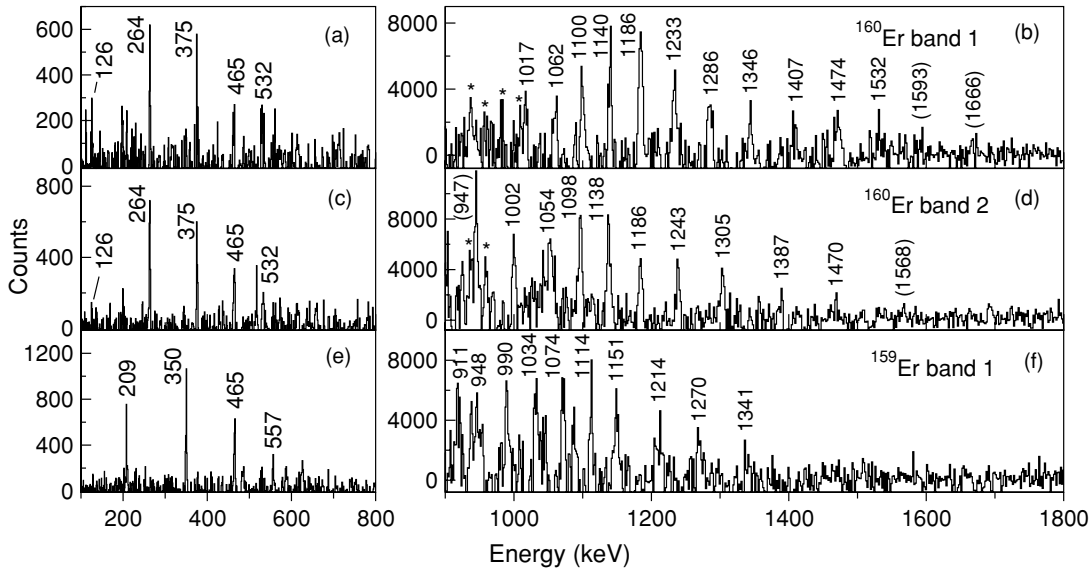

FIG. 1. Background-subtracted γ-ray spectra produced with sums of triple gates (a), (c), and (e) from the hypercube (E^4_γ) and double gates (b), (d), and (f) from the cube (E^3_γ) set on all of the firm transitions within the new rotational sequences associated with ^{160}Er and ^{159}Er. Transitions are labeled by their energies in keV. Photopeaks labeled in (a) and (c) correspond to the yrast γ decay of ^{160}Er [26] and photopeaks labeled in (e) correspond to the yrast γ decay of ^{159}Er [26]. Photopeaks labeled with asterisks in (b) and (d) correspond to transitions within the ^{160}Er yrast band. See text for further details.

to the decay of the $I^{\pi} = 30^{+}$, 32^{+}, 34^{+}, and 36^{+} yrast states, respectively [26,27]. These observations give strong evidence that this band is associated with ^{160}Er and suggest that the lowest energy states depopulate spins of the order of $35\hbar$.

A second rotational structure associated with the γ decay of ^{160}Er (band 2) has also been found in the present data. This weakly populated sequence comprises of nine γ-ray transitions from 1002 to 1470 keV and two tentative transitions at 947 and 1568 keV. A γ-ray spectrum produced with a sum of double gates placed on the transitions within the band is presented in Fig. 1(d) alongside the low-energy range of a γ-ray spectrum produced with a sum of triple gates, also set on these transitions, which shows the low-lying yrast transitions of ^{160}Er [Fig. 1(c)]. Photopeaks labeled with an asterisk in Fig. 1(d) at 938 and 960 keV correspond to the decays from the $I^{\pi} = 30^{+}$ and 32^{+} yrast states of ^{160}Er, respectively, which may also indicate that the lowest energy states depopulate spins of the order of $33\hbar$.

A third rotational structure consisting of ten transitions from 911 to 1341 keV was observed and is associated with ^{159}Er. This rotational structure is seen in the γ-ray spectrum of Fig. 1(f), which was produced with a sum of double gates placed on the all ten transitions. Figure 1(e) indicates that the low-lying transitions in the yrast band of ^{159}Er are in coincidence with the new band.

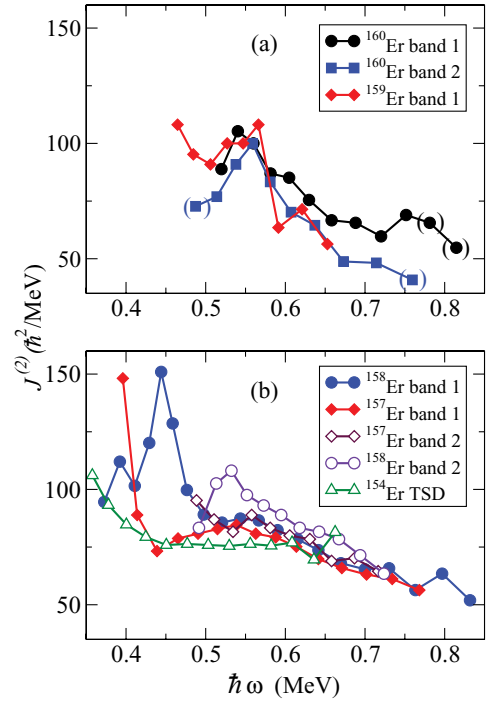

FIG. 2. (Color online) The dynamic moment of inertia $J^{(2)}$ as a function of rotational frequency $\hbar\omega$ for (a) the new bands associated with ^{159,160}Er and (b) proposed TSD bands in ^{157,158}Er [1], and the TSD band in ^{154}Er [11]. The parentheses are associated with tentative transitions.

IV. DISCUSSION

Under the assumption that the in-band transitions are of stretched E2 character, the dynamic moment of inertia, $J^{(2)}$, of the bands can be extracted. These quantities are plotted as a function of the rotational frequency $\hbar\omega$ in Fig. 2(a). For comparison, the $J^{(2)}$ values for the candidate TSD bands in ^{157,158}Er [1] and the TSD band in ^{154}Er [11] are plotted in Fig. 2(b). Detailed analysis of the dynamic moments of inertia have proved useful in understanding the behavior of highly collective structures such as those associated with superdeformation (see Refs. [28] and [29] and references therein). This work aims to apply the same methodology to this new class of ultrahigh-spin collective sequences in the erbium isotopes.

The $J^{(2)}$ moments of inertia for the new bands in ^{159,160}Er all decrease with increasing rotational frequency. This is consistent with the previously observed bands in ^{157,158}Er, which suggests a similar underlying intrinsic structure. The bands in ^{159,160}Er and band 2 in ^{158}Er display a rise or "bump" in the $J^{(2)}$ value with a maximum at $\sim$0.55 MeV. In addition, the bands in ^{159,160}Er are not observed much below $\sim$0.5 MeV; therefore, the possible existence of a sharp increase in the $J^{(2)}$ moment of inertia, seen at lower rotational frequencies in bands 1 in ^{157}Er and ^{158}Er, could not be established, although a rise in the $J^{(2)}$ moment of inertia at low rotational frequency is observed in ^{159}Er.

To achieve an understanding of the nature of the underlying structure of these bands, calculations have been performed within the framework of the configuration-dependent, cranked Nilsson-Strutinsky formalism without pairing [30,31].

In these calculations, the modified oscillator parameters are those used in Ref. [32] and references therein, that is, the so-called $A = 150$ parameters that have been used in all CNS calculations in this mass region over the past 20 years. The Lublin Strasbourg drop model [33] is used for the macroscopic energy with the rigid-body moment of inertia calculated with a radius parameter $r_0 = 1.16$ fm and a diffuseness parameter $a = 0.6$ fm [34]. Representative potential energy surfaces (PES) as a function of angular momentum with (parity, signature) $+ (\pi, \alpha) = (-, 1)$ for ^{160}Er from $31\hbar$ to $81\hbar$ are displayed in Fig. 3. Similar behavior is also found for the other (π, α) configurations in ^{160}Er and in ^{159}Er. The triaxiality parameter γ, used in the polar description of rotating quadrupole shapes, is defined by the Lund convention [9].

The PESs shown in Fig. 3 indicate a wide variety of nuclear shapes that compete for yrast status as a function of angular momentum. The various minima of interest in the PESs are labeled 1–7 in Fig. 3. At low spin, Fig. 3(a), the lowest-energy minimum in the PES corresponds to a well-developed prolate shape at $\gamma = 0^{\circ}$ and $\varepsilon_2 \sim 0.23$, labeled 1. As the angular momentum is increased, this minimum migrates across the γ plane toward an oblate (or near oblate) noncollective structure ($\gamma = 60^{\circ}$), labeled 4 in Fig. 3(c). For low and medium spin values, two minima are present at $\varepsilon_2 \sim 0.37$ and $\gamma \sim \pm 20^{\circ}$, labeled 2 and 3, respectively, corresponding to TSD shapes.

At high spins ($51\hbar$–$81\hbar$) another minimum at $\varepsilon_2 \sim 0.45$, $\gamma \sim 20^{\circ}$, labeled 5 in Fig. 3(f), is calculated to become yrast at $\sim 71\hbar$. A small minimum is also predicted to occur at $\varepsilon_2 \sim 0.28$, $\gamma \sim 5^{\circ}$, labeled 6 [Fig. 3(d)], between $\sim 51\hbar$ and

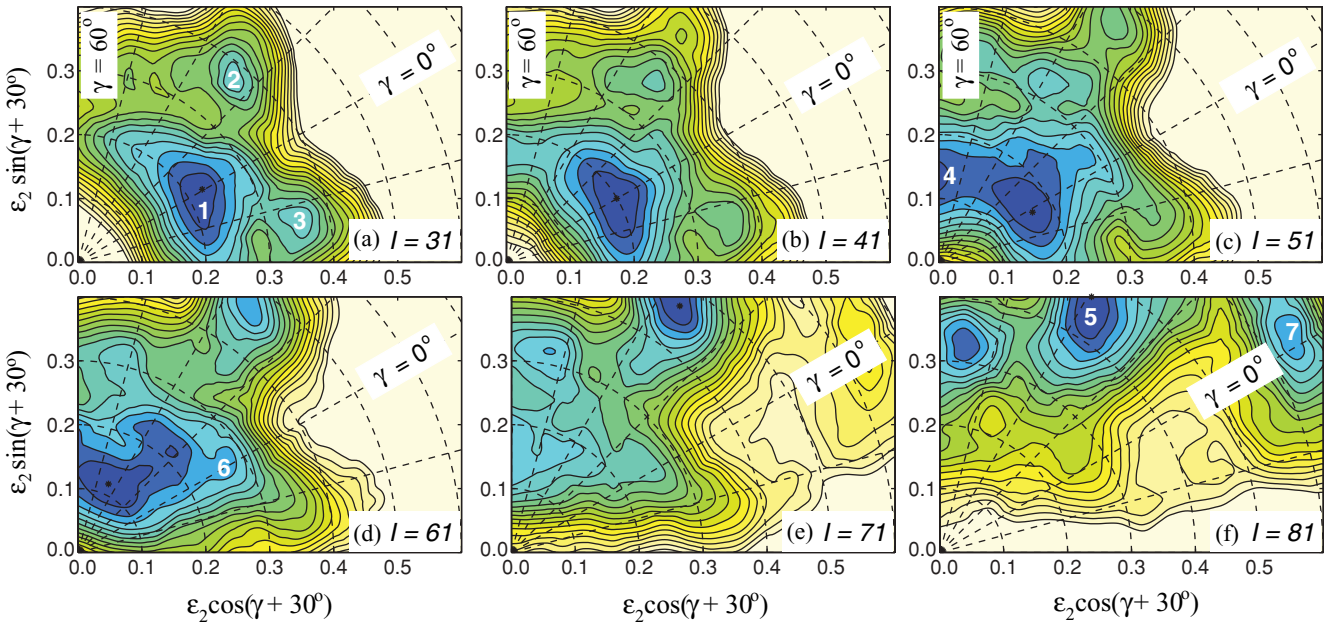

FIG. 3. (Color online) Calculated potential-energy surfaces versus quadrupole deformation ε_2 and the triaxiality parameter γ of ^{160}Er with $(\pi, \alpha) = (-, 1)$ for spins $I = 31, 41, 51, 61, 71$, and 81, labeled (a)–(f), respectively. Contour lines are separated by 0.25 MeV and the γ plane is marked at 15° intervals. Dark regions represent low energy with absolute minima labeled with a dot. Individual minima labeled 1–7 are discussed in the text.

71$\hbar$. At the very highest spins, highly deformed prolate shapes are predicted to occur before the onset of fission [9], and such a minimum is seen to be established in the PES at 81$\hbar$, labeled 7. The dynamic moment of inertia values extracted for these minima (5, 6, and 7) do not compare favorably with the values for the new experimentally observed bands. Furthermore, the energy for minima 5 and 7 are calculated to be too high in excitation energy at lower spin (40$\hbar$–50$\hbar$) to result in detectable γ-ray yields. Therefore, these minima are not discussed further.

A. The TSD minima at $\varepsilon_2 \sim 0.37$ and $\gamma \sim \pm 20°$

A possible interpretation for the new bands in ^{159,160}Er is that they are associated with the minima at $\varepsilon_2 \sim 0.37$ and $\gamma \sim \pm 20°$, labeled 2 and 3, respectively, in Fig. 3(a), similar to those suggested for ^{157,158}Er [1]. Quantitative energy calculations have, therefore, been carried out for these minima. The extracted configurations are labeled relative to the ^{146}Gd ($Z = 64$, $N = 82$) closed core; that is,

$$\pi(h_{11/2})^{p_1}(h_{9/2}f_{7/2})^{p_2}(i_{13/2})^{p_3} \ldots \nu(N_{\rm osc} = 4)^{-n_1}(h_{11/2})^{-n_2}(i_{13/2})^{n_3},$$

specifying the number of particles and holes in orbitals outside the core. The number of protons in the $N_{\rm osc} = 4$ orbitals and neutrons in the $h_{9/2}f_{7/2}$ orbitals is then fixed from the particle numbers, $Z = 68$, $N = 92$ (or 91 for ^{159}Er), respectively. For convenience, the configurations will be given in the shorthand notation, $[p_1(p_2p_3), (n_1n_2)n_3]$, where the numbers in parentheses are given only when they are different from zero.

1. Positive-γ configurations

For the positive-γ minimum (at $\varepsilon_2 \sim 0.37, \gamma \sim 20°$) calculated excitation energies for six low-energy configurations in ^{160}Er are plotted, relative to that of a rotating liquid drop [34], as a function of spin in Fig. 4(a). The associated dynamic moments of inertia are given as a function of rotational frequency in Fig. 4(b). To understand the single-particle occupancy given in Fig. 4 for these configurations, the single-particle Routhians are plotted for protons and neutrons in Figs. 5(a) and 5(b), respectively.

The favored proton configuration above $\hbar\omega \sim 0.4$ MeV [see Fig 5(a)] is the negative-parity configuration,

$$\pi(h_{11/2})^6(h_{9/2}f_{7/2})^1(i_{13/2})^1,$$

or [6(11)] in the shorthand notation. For neutrons [Fig. 5(b)], an energy gap appears for $N = 90$ that remains over a large frequency range. The lowest $N = 92$ configurations can be formed by filling two of the four $h_{9/2}f_{7/2}$ or $i_{13/2}$ orbitals above this gap, resulting in six different configurations.

It is the combination of these six neutron configurations with the favored proton configuration that forms the low-energy triaxial structures. Note that all these neutron configurations have the typical feature of the triaxial structures in this region of the nuclear chart, for example, two neutron holes in both the $N_{\rm osc} = 4$ and $h_{11/2}$ orbitals [1].

The resulting six configurations can be split into two distinct groups, those that show a bump in the $J^{(2)}$ moment of inertia at ~0.45–0.50 MeV [Fig. 4(b)] and those that do not exhibit this anomaly, but experience a sharp discontinuity at ~0.75 MeV. The bump at ~0.45 MeV in the $J^{(2)}$ moment of inertia is associated with an alignment involving a pair

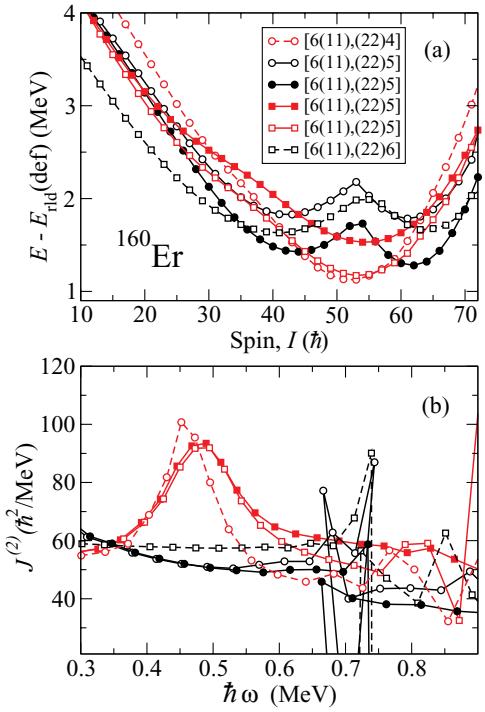

FIG. 4. (Color online) (a) Calculated excitation energies E relative to that of a rotating liquid drop $E_{\rm rld}$ as a function of spin I for the six lowest-energy, positive-γ configurations ($\varepsilon_2 = 0.37$, $\gamma \sim 20^\circ$) and (b) $J^{(2)}$ values as a function of rotational frequency $\hbar\omega$ for the six low-lying collective configurations in ^{160}Er. Solid lines correspond to positive parity configurations and broken lines correspond to negative parity. Similarly, solid symbols correspond to positive signature and open symbols correspond to negative signature.

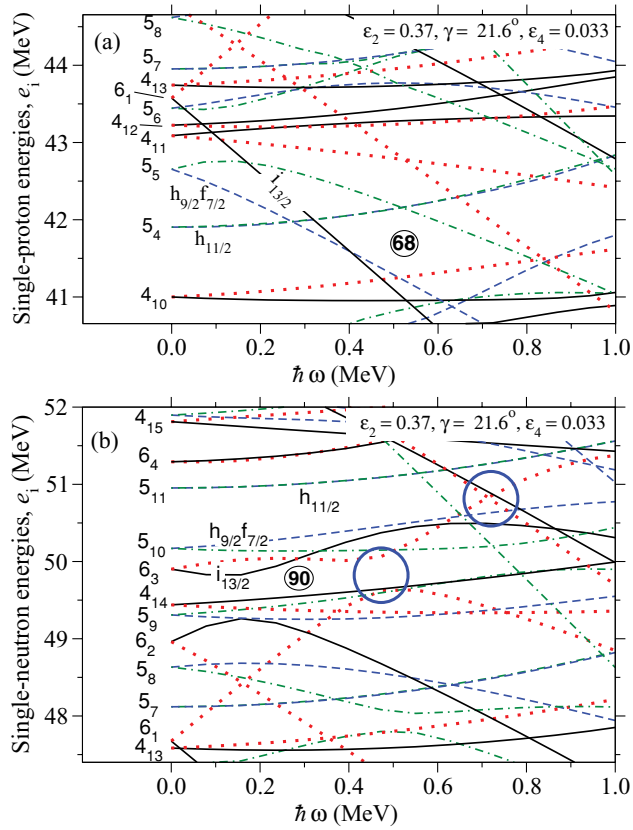

FIG. 5. (Color online) Single-particle proton (a) and neutron (b) energies as a function of rotational frequency (Routhians) at a deformation of $\varepsilon_2 = 0.37$, $\gamma \sim 20^\circ$. The orbitals are labeled at $\hbar\omega = 0$ by the $N_{\rm osc}$ shell (sometimes referred to as $N_{\rm rot}$ shell [31]) to which they belong with the ordering within the N shell as a subscript. A few orbitals important for the present interpretation are also labeled in a similar way by their dominating j shell(s). The line types distinguish between different (π, α) combinations: solid lines represent $(+,+1/2)$, dotted lines $(+,-1/2)$, dashed lines $(-,+1/2)$, and dash-dotted lines $(-,-1/2)$. The areas marked with circles refer to specific issues discussed in the text.

of $i_{13/2}$ neutrons, as indicated with a circle in Fig. 5(b). The two new experimentally observed bands associated with ^{160}Er exhibit a bump in the $J^{(2)}$ moment of inertia at $\sim$0.55 MeV [Fig. 6(a)]. Therefore, in this scenario, the observed bump may be attributed to this $i_{13/2}$ neutron alignment. If the third $N_{\rm osc} = 6$ $\alpha = -1/2$ orbital is occupied, see Fig. 5(b), then the strong alignment at 0.45 MeV is effectively blocked and a crossing with a down-sloping $i_{11/2}/g_{9/2}$ orbital at $\sim$0.75 MeV is predicted, which is also indicated by a circle in Fig. 5(b). The [6(11), (22)5] and [6(11), (22)4] configurations follow the trends of the $J^{(2)}$ moment of inertia for the experimentally observed bands in ^{160}Er. This is demonstrated in Fig. 6(a) where the configurations that have the best overall agreement, namely the two [6(11), (22)5] signatures, are compared with the data.

For ^{159}Er, the favored proton configurations are the same as for ^{160}Er in the positive-γ minima. The favored neutron configurations are formed with one of the four $h_{9/2}f_{7/2}$ and $i_{13/2}$ orbits above the $N = 90$ shell gap filled in the single-particle Routhians of Fig. 5(b). Figure 6(b) displays three of the four configurations that have characteristics similar to the observed band. The same $i_{13/2}$ neutron alignment also appears present in ^{159}Er. In both ^{159}Er and ^{160}Er, this alignment occurs at a slightly higher rotational frequency in the experiment than is predicted. This difference is not unreasonable in view of the uncertainties in the calculations, where the crossing frequency is very sensitive to changes in deformation and residual pairing might play a role as well.

It is interesting to note that, in the lighter $N = 86$ isotope ^{154}Er, the bump at $\sim$0.55 MeV is not present [see Fig. 2(b)]. This indicates that the $i_{13/2}$ neutron orbitals involved are not active, which is consistent with them being further in energy from the Fermi surface.

Based on the interpretation that the observed bands correspond to the $\varepsilon_2 \sim 0.37$, $\gamma \sim 20^\circ$ minimum, the calculations predict that the band in ^{159}Er extends to $I \sim 97/2$ and the bands in ^{160}Er extend to $I \sim 59$ and $I \sim 55$ for bands 1 and 2, respectively. These assignments are consistent with the observation of yrast decays in ^{160}Er occurring around $I^\pi \sim 36^+$ in the γ-ray spectra.

2. *Negative-γ configurations*

Recent lifetime measurements [35] for the candidate TSD bands observed in ^{157,158}Er have determined that these

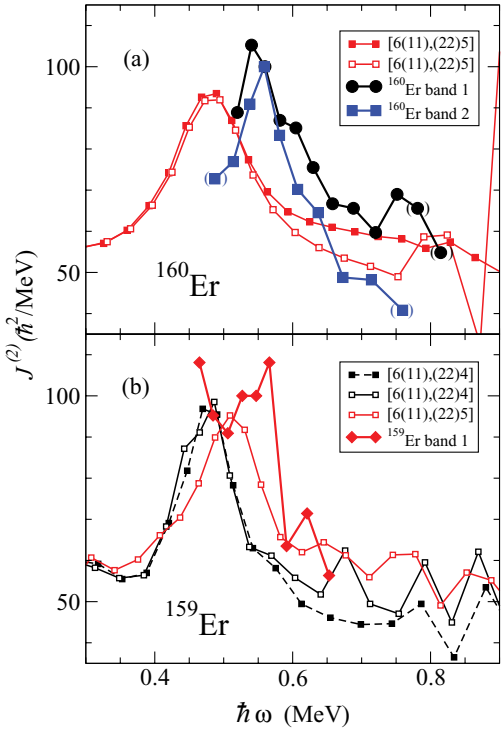

FIG. 6. (Color online) Theoretical (positive γ) and experimental dynamic moments of inertia $J^{(2)}$ as a function of rotational frequency $\hbar\omega$ for ^{160}Er (a) and ^{159}Er (b). The parentheses are associated with tentative transitions.

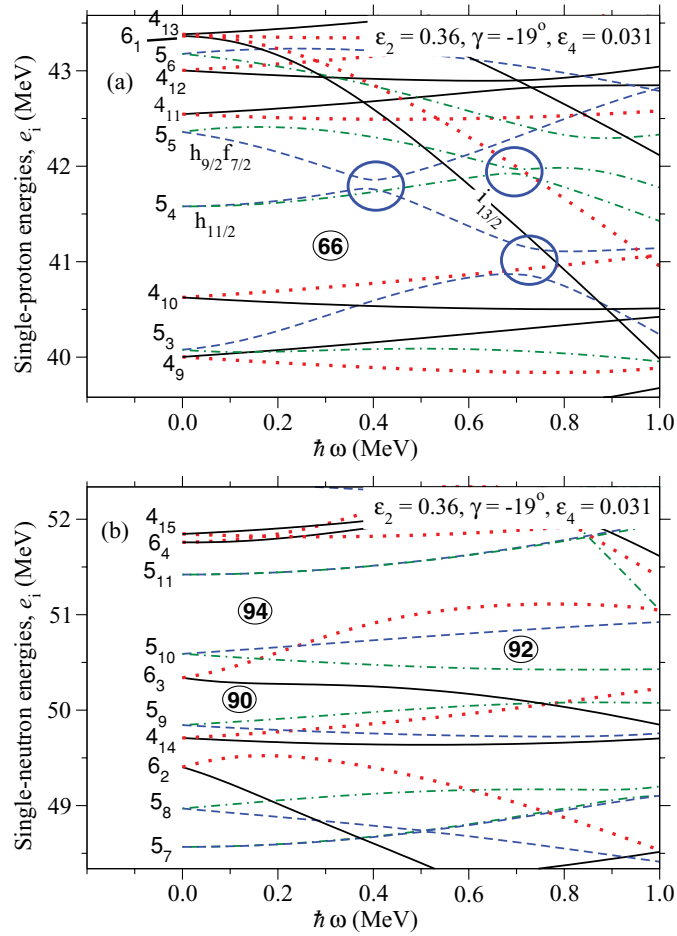

FIG. 7. (Color online) Single-particle proton (a) and neutron (b) energies as a function of rotational frequency (Routhians) at a deformation of $\varepsilon_2 = 0.36$, $\gamma = -19°$. The orbitals are labeled using the same convention as described in the caption of Fig. 5.

structures are indeed associated with large quadrupole moments. These measurements indicate, however, that the bands are strongly deformed and most compatible with negative-γ deformation. Therefore, to consider this possibility, the configurations that arise from the minimum in the PES plots for ^{160}Er at negative γ ($\varepsilon_2 \sim 0.37$, $\gamma \sim -20°$) [labeled 3 in Fig. 3(a)] have also been investigated in detail.

Single-particle Routhians at a deformation typical for this negative triaxial minimum are plotted for protons and neutrons in Figs. 7(a) and 7(b), respectively. A comparison between the proton orbitals of Fig. 7(a) and the corresponding proton orbitals at positive γ [Fig. 5(a)] indicates that there are common crossings between the 5_4 $h_{11/2}$ orbital and the 5_5 $h_{9/2}f_{7/2}$ orbital of each signature, which are marked with circles in Fig. 7(a) at $\hbar\omega \sim 0.40$, $\sim$0.70, and $\sim$0.75 MeV. For negative γ, these orbitals interact strongly; therefore, in the calculations, the adiabatic path of the orbitals is followed through the crossings. Consequently, the configuration-labeling notation will change after each crossing. This is contrary to the positive-γ situation, where the interactions are much smaller and the diabatic path of the orbitals is followed. Therefore, for negative-γ deformation, the bands are labeled according to their configuration over the spin range of the experimentally observed bands [0.5–0.6 MeV in Fig. 7(a)]. The favored proton configurations are then either [7(10)] or [6(11)]. Similar types of crossing have previously been observed in the SD bands of $^{146-148}$Gd ($N_{\rm osc} = 6$ orbitals) [36] and ^{140}Nd ($N_{\rm osc} = 5$ orbitals) [37].

The favored neutron configurations are predicted to be similar to those for positive-γ deformation. However, in contrast to positive-γ deformation [Fig. 5(b)] for the neutrons, there are no crossings within the $N_{\rm osc}$ shells for the valence orbitals.

The calculated excitation energies and $J^{(2)}$ moment of inertia for five low-energy, negative-γ configurations at $\varepsilon_2 \sim 0.36$ are given in Figs. 8(a) and 8(b), respectively. The two signatures of the low-energy, positive-γ [6(11),(22)5] configuration are also given for comparison. It can be seen that the negative-γ configurations are competitive in energy for all spin values and that some of these are favored at low spin. If band 1 in ^{160}Er is assigned to the [6(11),(22)5] negative-γ configuration, which is favored at high spin, then the predicted spin range is similar or possibly slightly higher than predicted for positive-γ deformation.

The bump observed at 0.55 MeV in the $J^{(2)}$ moment of inertia for the experimental data (Fig. 2) can be compared with the calculated bumps at $\sim$0.4–0.5 MeV [see Fig. 8(b)]. These correspond to a crossing involving the $N_{\rm osc} = 5$ $h_{11/2}$ and $h_{9/2}f_{7/2}$ proton orbitals, marked in Fig. 7(a). However, the calculated bump is much more sharply peaked than that

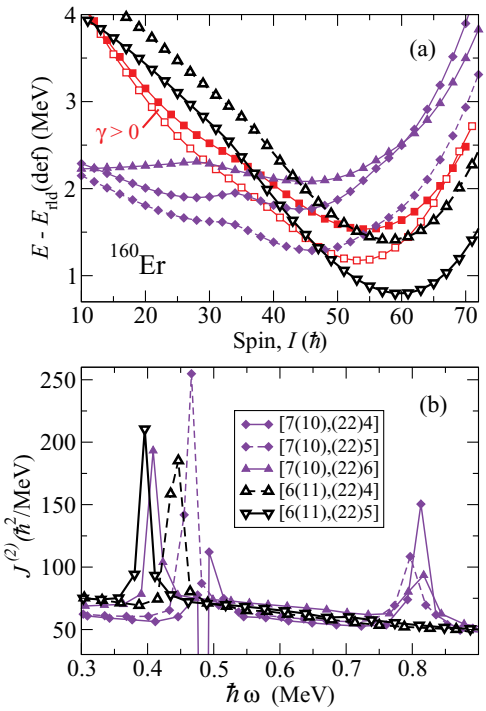

FIG. 8. (Color online) (a) Calculated excitation energies relative to that of a rotating liquid drop as a function of spin for the five lowest-energy, negative-γ configurations ($\varepsilon_2 = 0.37, \gamma \sim -20^\circ$). Two low-energy, positive-γ configurations (shown in red) from Fig. 6(a) are included for comparison. (b) $J^{(2)}$ moments of interia as a function of rotational frequency for low-lying, negative-γ collective configurations in ^{160}Er.

observed in ^{160}Er. This would suggest it unlikely that the experimental bump is caused by a crossing within the $N_{\rm osc} = 5$ proton orbitals. Indeed, the calculated bump is rather similar to that observed in the TSD candidate band 1's of ^{158}Er and ^{157}Er [Fig. 2(b)]. However, the bands in ^{160}Er (and ^{159}Er) are not observed to sufficiently low frequency to test if such a sharply peaked bump also occurs in these bands. In addition, the calculated bump for the different bands is spread over a rather large frequency range. This spread is caused by the different deformations associated with the different configurations, which illustrates how sensitive these crossings are to deformation changes. It it also interesting to note that the sharpness of the bump in the $J^{(2)}$ is related to the interaction strength and to the degree of mixing between the configurations. This will be sensitive to the pairing strength, which is not included in these calculations.

For ^{159}Er, the negative-γ minimum proton configurations are the same as for ^{160}Er and, therefore, the general conclusions about the interpretation of the bands in ^{160}Er can also be applied to the band observed in ^{159}Er.

V. CONCLUSIONS

Three high-spin rotational bands with high dynamic moments of inertia have been observed in the present work, two in ^{160}Er and one in ^{159}Er. The striking similarity with recently discovered rotational sequences in other Er isotopes suggests the same underlying structure. Cranked Nilsson-Strutinsky calculations without pairing suggest that the sequences correspond to triaxial structures with $\varepsilon_2 \sim 0.37$ and $\gamma \sim \pm 20^\circ$ and extend up to spin of $\sim 60\hbar$. Configurations with both positive- and negative-γ triaxial deformation offer possible interpretations of the experimentally observed dynamic moment of inertia characteristics. Although there is better overall agreement for the positive-γ configurations, the current data cannot distinguish between these two interpretations and a fully consistent picture has yet to emerge. This points to the importance of performing lifetime measurements for these bands. In addition, it would be interesting to identify both positive and negative triaxial deformed bands in the same nucleus in this region.

ACKNOWLEDGMENTS

We thank Paul Morrall from STFC Daresbury Laboratory for preparing the targets and the staff at Argonne National Laboratory for their excellent support. This work is supported by the United Kingdom Science and Technology Facilities Council, the State of Florida, the National Science Foundation under Contract No. PHY-0554762, the US Department of Energy, Office of Nuclear Physics, under Contract Nos. DE-AC02-06CH11357 and DE-FG02-96ER40963, and the Swedish Science Research Council.

[1] E. S. Paul, P. J. Twin, A. O. Evans, A. Pipidis, M. A. Riley, J. Simpson, D. E. Appelbe, D. B. Campbell, P. T. W. Choy, R. M. Clark *et al.*, Phys. Rev. Lett. **98**, 012501 (2007).

[2] P. J. Twin, B. M. Nyakó, A. H. Nelson, J. Simpson, M. A. Bentley, H. W. Cranmer-Gordon, P. D. Forsyth, D. Howe, A. R. Mokhtar, J. D. Morrison *et al.*, Phys. Rev. Lett. **57**, 811 (1986).

[3] P. Bringel, H. Hübel, A. Al-Khatib, A. Bürger, N. Nenoff, A. Neußer-Neffgen, G. Schönwasser, A. K. Singh, G. B. Hagemann, B. Herskind *et al.*, Phys. Rev. C **73**, 054314 (2006).

[4] S. W. Ødegård, G. B. Hagemann, D. R. Jensen, M. Bergström, B. Herskind, G. Sletten, S. Törmänen, J. N. Wilson, P. O. Tjøm, I. Hamamoto *et al.*, Phys. Rev. Lett. **86**, 5866 (2001).

[5] D. R. Jensen, G. B. Hagemann, I. Hamamoto, S. W. Ødegård, B. Herskind, G. Sletten, J. N. Wilson, K. Spohr, H. Hübel, P. Bringel *et al.*, Phys. Rev. Lett. **89**, 142503 (2002).

[6] G. Schönwaßer, H. Hübel, G. B. Hagemann, P. Bednarczyk, G. Benzoni, A. Bracco, P. Bringel, R. Chapman, D. Curien, J. Domscheit *et al.*, Phys. Lett. **B552**, 9 (2003).

[7] H. Amro, W. C. Ma, G. B. Hagemann, R. M. Diamond, J. Domscheit, P. Fallon, A. Görgen, B. Herskind, H. Hübel, D. R. Jensen *et al.*, Phys. Lett. **B553**, 197 (2003).

[8] A. Bohr and B. R. Mottelson, *Nuclear Structure* (W. A. Benjamin Inc., New York, 1975), Vol. II, and references therein.

[9] G. Andersson, S. E. Larsson, G. Leander, P. Möller, S. G. Nilsson, I. Ragnarsson, S. Åberg, R. Bengtsson, J. Dudek, B. Nerlo-Pomorska *et al.*, Nucl. Phys. **A268**, 205 (1976).

[10] L. A. Bernstein, J. R. Hughes, J. A. Becker, L. P. Farris, E. A. Henry, S. J. Asztalos, B. Cederwall, R. M. Clark, M. A. Deleplanque, R. M. Diamond *et al.*, Phys. Rev. C **52**, R1171 (1995).

[11] K. Lagergren, B. Cederwall, T. Bäck, R. Wyss, E. Ideguchi, A. Johnson, A. Ataç, A. Axelsson, F. Azaiez, A. Bracco *et al.*, Phys. Rev. Lett. **87**, 022502 (2001).

[12] A. Aguilar, D. B. Campbell, K. Chandler, A. Pipidis, M. A. Riley, C. Teal, J. Simpson, D. J. Hartley, F. G. Kondev, R. M. Clark *et al.* Phys. Rev. C **77**, 021302(R) (2008).

[13] C. Teal, K. Lagergren, A. Aguilar, M. A. Riley, J. Simpson, M. P. Carpenter, U. Garg, D. J. Hartley, R. V. F. Janssens, D. T. Joss *et al.*, Phys. Rev. C **78**, 017305 (2008).

[14] N. S. Pattabiraman, Y. Gu, S. Frauendorf, U. Garg, T. Li, B. K. Nayak, X. Wang, S. Zhu, R. V. F. Janssens, R. S. Chakrawarthy *et al.*, Phys. Lett. **B647**, 243 (2007).

[15] X. Wang, R. V. F. Janssens, E. F. Moore, U. Garg, Y. Gu, S. Frauendorf, M. P. Carpenter, S. S. Ghugre, N. J. Hammond, T. Lauritsen *et al.*, Phys. Rev. C **75**, 064315 (2007).

[16] H. Amro, P. G. Varmette, W. C. Ma, B. Herskind, G. B. Hagemann, G. Sletten, R. V. F. Janssens, M. Bergström, A. Bracco, M. Carpenter *et al.*, Phys. Lett. **B506**, 39 (2001).

[17] A. Neußer-Neffgen, H. Hübel, P. Bringel, J. Domscheit, E. Mergel, N. Nenoff, A. K. Singh, G. B. Hagemann, D. R. Jensen, S. Bhattacharya *et al.*, Phys. Rev. C **73**, 034309 (2006).

[18] Y. C. Zhang, W. C. Ma, A. V. Afanasjev, G. B. Hagemann, J. Begnaud, M. P. Carpenter, P. Chowdhury, D. M. Cullen, M. K. Djongolov, D. J. Hartley *et al.*, Phys. Rev. C **76**, 064321 (2007).

[19] D. J. Hartley, M. K. Djongolov, L. L. Riedinger, G. B. Hagemann, R. V. F. Janssens, F. G. Kondev, E. F. Moore, M. A. Riley, A. Aguilar, C. R. Bingham *et al.*, Phys. Lett. **B608**, 31 (2005).

[20] D. T. Scholes, D. M. Cullen, F. G. Kondev, R. V. F. Janssens, M. P. Carpenter, D. J. Hartley, M. K. Djongolov, G. Sletten, G. Hagemann, C. Wheldon *et al.*, Phys. Rev. C **70**, 054314 (2004).

[21] R. B. Yadav, W. C. Ma, G. B. Hagemann, R. Bengtsson, H. Ryde, H. Amro, A. Bracco, M. P. Carpenter, J. Domscheit, S. Frattini *et al.*, Phys. Rev. C **78**, 044316 (2008).

[22] J. Simpson, AIP Conf. Proc. **1072**, 136 (2008).

[23] M. A. Riley, A. Aguilar, A. O. Evans, D. J. Hartley, K. Lagergren, J. Ollier, E. S. Paul, A. Pipidis, J. Simpson, C. Teal, P. J. Twin, X. Wang, D. E. Appelbe, D. B. Campbell, M. P. Carpenter, R. M. Clark, M. Cromaz, I. G. Darby, P. Fallon, U. Garg, R. V. F. Janssens, D. T. Joss, F. G. Kondev, T. Lauritsen, I. Y. Lee, C. J. Lister, A. O. Macchiavelli, P. J. Nolan, M. Petri, S. V. Rigby, J. Thompson, C. Unsworth, D. Ward, S. Zhu, and I. Ragnarsson, Acta Phys. Pol. B **40**, 513 (2009).

[24] I. Y. Lee, Nucl. Phys. **A520**, 641c (1990).

[25] D. C. Radford, Nucl. Instrum. Methods Phys. Res. A **361**, 297 (1995).

[26] J. Simpson, M. A. Riley, A. N. James, A. R. Mokhtar, H. W. Cranmer-Gorden, P. D. Forsyth, A. J. Kirwan, D. Howe, J. D. Morrison, and J. F. Sharpey-Schafer, J. Phys. G **13**, L235 (1987).

[27] F. G. Kondev, M. A. Riley, J. Simpson, R. V. F. Janssens, A. V. Afanasjev, I. Ragnarsson, T. B. Brown, D. J. Hartley, M. P. Carpenter, P. Fallon *et al.*, J. Phys. G **25**, 897 (1999).

[28] P. J. Nolan and P. Twin, Annu. Rev. Nucl. Part. Sci. **38**, 533 (1988).

[29] R. V. F. Janssens and T. L. Khoo, Annu. Rev. Nucl. Part. Sci. **41**, 321 (1991).

[30] A. V. Afanasjev, D. B. Fossan, G. J. Lane, and I. Ragnarsson, Phys. Rep. **322**, 1 (1999).

[31] T. Bengtsson and I. Ragnarsson, Nucl. Phys. **A436**, 14 (1985).

[32] T. Bengtsson, Nucl. Phys. **A512**, 124 (1990).

[33] K. Pomorski and J. Dudek, Phys. Rev. C **67**, 044316 (2003).

[34] B. G. Carlsson and I. Ragnarsson, Phys. Rev. C **74**, 011302(R) (2006).

[35] X. Wang *et al.* (private communication).

[36] B. Haas, V. Janzen, D. Ward, H. Andrews, D. Radford, D. Prévost, J. Kuehner, A. Omar, J. Waddington, T. Drake *et al.*, Nucl. Phys. **A561**, 251 (1993).

[37] A. Neußer, H. Hübel, A. Al Khatib, P. Bringel, A. Bürger, N. Nenoff, G. Schönwaßer, A. K. Singh, C. M. Petrache, G. L. Bianco *et al.*, Phys. Rev. C **70**, 064315 (2004).